Supporting Information

Gradient Phosphorus-Doping Engineering and Superficial Amorphous Reconstruction in $NiFe_2O_4$ Nanoarray to Enhance Oxygen Evolution Electrocatalysis

Wei Zong,[‡a] Dewei Rao,[‡c] Hele Guo,[a] Yue Ouyang,[a] Yue-E Miao,[a] Wei Wang,[d] Jing Wang,[e] Feili Lai,[*a] and Tianxi Liu[*a]

[a]State Key Laboratory for Modification of Chemical Fibers and Polymer Materials, College of Materials Science and Engineering, Innovation Center for Textile Science and Technology, Donghua University, Shanghai 201620, P. R. China
Email: txliu@dhu.edu.cn

[b]Department of Chemistry, KU Leuven, Celestijnenlaan 200F, Leuven 3001, Belgium
Email: feili.lai@kuleuven.be

[c]School of Materials Science and Engineering, Jiangsu University, Zhenjiang, Jiangsu 212013, P. R. China

[d]Beijing Key Laboratory of Bio-inspired Energy Materials and Devices, School of Space and Environment, Beihang University, Beijing, 100191 PR, China

[e]School of Chemical Engineering and Energy, Zhengzhou University, Zhengzhou, Henan 450001, P. R. China

[‡] These authors contributed equally to this work.

S-1. Synthesis Methods

1.1 Materials

Polyacrylonitrile (PAN) (M_w = 130000 g mol^{-1}) was purchased from Sigma-Aldrich. *N, N*-dimethylformamide (DMF), iron nitrate nonahydrate ($Fe(NO_3)_3 \cdot 9H_2O$), nickel nitrate hexahydrate ($Ni(NO_3)_2 \cdot 6H_2O$), cobaltous nitrate hexahydrate ($Co(NO_3)_2 \cdot 6H_2O$), ammonium fluoride (NH_4F, ≥ 99.9%), urea ($CO(NH_2)_2$), sodium hypophosphite monohydrate ($NaH_2PO_2 \cdot H_2O$, ≥ 99%), were all purchased from Sinopharm Chemical Reagent Co. Ltd. All the other reagents were purchased from Sinopharm Chemical Reagent Co. Ltd. All the chemicals were used as received without further purification.

1.2 Preparation of nitrogen-doped carbon nanofibers

The PAN nanofiber was firstly prepared by a facile single-nozzle electrospinning technique using a commercial electrospinning system (UCALERY Beijing Co. Ltd., China). Typically, 1 g PAN was dissolved in 9 g DMF solvent at room temperature to form a homogeneous precursor solution. During the electrospinning process, it was carried out at a high voltage of 20 kV at a feeding rate of 0.12 mm min^{-1} through a stainless needle. Then, the pre-oxidized treatment of the PAN membrane was prepared at 250 °C in air atmosphere for 1 h with a heating rate of 1 °C min^{-1}. The carbonization was carried out under a nitrogen atmosphere at 800 °C for 2 h with a heating rate of 5 °C min^{-1}, denoted as nitrogen-doped carbon nanofibers (NCNF).

1.3 Synthesis of OP-$NiFe_2O_4$/NCNF

Typically, $Ni(NO_3)_2 \cdot 6H_2O$ (0.5 mmol), $Fe(NO_3)_3 \cdot 9H_2O$ (1.0 mmol), NH_4F (5 mmol), and urea (10 mmol) were dissolved in H_2O (30 ml). One piece of nitrogen-doped carbon nanofiber (2 × 2 cm^2) is immersed in the above solution. The mixed solution was then sealed in a 100 ml Teflon-lined stainless-steel autoclave and heated at 120 °C for 10 hours. After washed with distilled water and absolute ethanol, the NiFe-LDH nanoarray on nitrogen-doped carbon nanofibers (NiFe-LDH/NCNF) were obtained. The prepared NiFe-LDH/NCNF was followed by an annealing treatment at 350 °C for 2 h in N_2 atmosphere to get the $NiFe_2O_4$ nanoarray on NCNF ($NiFe_2O_4$/NCNF). The $NiFe_2O_4$/NCNF and NaH_2PO_2 were placed into two separate positions in a porcelain boat, in which NaH_2PO_2 was placed on the upstream side of the furnace to get the phosphorus-doped $NiFe_2O_4$ nanoarray on NCNF (P-$NiFe_2O_4$/NCNF). The process of electrochemical activation was performed in oxygen-saturated 1 M KOH solution. The CV tests were carried out from 0.1 to 0.8 V *vs* Ag/AgCl at sweep rate of 50 mV s^{-1} of 1000 cycles. As a result, the superficial oxyhydroxide, phosphorus-doped $NiFe_2O_4$ nanoarray on NCNF (OP-$NiFe_2O_4$/NCNF) was prepared.

1.4 Synthesis of OP-$NiCo_2O_4$/NCNF and OP-$CoFe_2O_4$/NCNF

Typically, $Ni(NO_3)_2 \cdot 6H_2O$ (0.5 mmol), $Co(NO_3)_2 \cdot 6H_2O$ (1 mmol) and methenamine (HMT) (4 mmol) were added into 30 mL of ethanol/water (v/v = 1 : 1) solution with a piece of NCNF membrane (2 × 2 cm^2) in the autoclave, and maintained at 80 °C for 8 h to get NiCo-LDH nanoarray on NCNF (NiCo-LDH/NCNF). The mixture of $Co(NO_3)_2 \cdot 6H_2O$ (0.5 mmol), $Fe(NO_3)_3 \cdot 9H_2O$ (1.0 mmol), NH_4F (5 mmol) and urea (10 mmol) were dissolved in H_2O (30 ml) with a piece of NCNF membrane (2 × 2 cm^2) in the autoclave and heated at 120 °C for 10 hours to get CoFe-LDH nanoarray on NCNF (CoFe-LDH/NCNF). Furthermore, the prepared precursors were followed by annealing at 350 °C for 2 h and further phosphatization at 300 °C for 1 h in N_2 atmosphere to get the phosphorus-doped $NiCo_2O_4$ nanoarray on NCNF (P-$NiCo_2O_4$/NCNF) and phosphorus-doped $CoFe_2O_4$ nanoarray on NCNF (P-$CoFe_2O_4$/NCNF), respectively. Finally, the superficial oxyhydroxide, phosphorus-doped $NiCo_2O_4$ nanoarray and $CoFe_2O_4$ nanoarray on NCNF (OP-$NiCo_2O_4$/NCNF and OP-$CoFe_2O_4$/NCNF) samples were prepared by the similar electrochemical activation process of OP-$NiCo_2O_4$/NCNF.

S-2. Electrochemical Measurements

All the electrochemical measurements were carried out on a CHI660B electrochemical workstation (CH Instruments, Inc., Shanghai) with a standard three-electrode system at room temperature. The homogeneous ink was prepared by adding 5 mg of the catalyst into a mixed solution of 95 μL of Nafion solution (5 wt%, Sigma Aldrich) and 350 μL of ethanol under sonication for 10 min. Then 3 μL of the catalyst ink was cast onto the glassy carbon electrode (diameter of 4 mm) and dried at room temperature. The OER performances were evaluated in O_2-saturated 1.0 M KOH solution by using Ag/AgCl electrode as the reference and a graphite rod as the counter electrode. The linear sweep voltammetry (LSV) was carried out at 10 mV s^{-1} to obtain the polarization curves and Tafel slopes. The double layer capacitance (C_{dl}) was used to evaluate the active surface areas, which the measured currents is in a relatively narrow potential window without faradaic reaction processes. Electrochemical impedance spectroscopy measurements (EIS) were performed using a CHI 660D electrochemistry working station by applying AC amplitude, with a frequency range from 100 kHz to 0.1 Hz with an amplitude of 5 mV. All polarization curves were corrected for IR drop throughout the system. Moreover, all potentials in this work were calibrated to corresponding potentials versus the RHE using the equation:

$$E_{(RHE)} = E_{Ag/AgCl} + 0.197 + 0.0591pH. \quad (1)$$

The turnover frequency (TOF; s^{-1}) for OER was calculated with the following equation:

$$TOF = I/(4Fn) \quad (2)$$

where I is the current (A), F is the Faraday constant (C mol^{-1}), and n is the number of active sites (mol). The factors of 1/4 are the corresponding electron transfer numbers.

Determination of generated oxygen. The volume of oxygen generated from the OER process in the presence of electrocatalysts was measured using a water-displacement method. In detail, the O_2 gas generated from the OER process at a constant current density of 10 mA cm^{-2}.

S-3. Characterizations

The morphology of the all samples were observed by field-emission scanning electron microscopy (FESEM, Ultra 55) and high-resolution transmission electron microscopy (HRTEM, Talos F200S). X-ray diffraction (XRD) patterns were measured using an X'Pert Pro X-ray diffractometer equipped with Cu Kα radiation (λ = 0.1542 nm) at a current of 40 mA and voltage of 40 kV. X-ray photoelectron spectroscopy (XPS) analyses were made with a VG ESCALAB 220I-XL device. The curve fitting of all XPS spectra was accomplished using XPS Peak 4.1 software. All XPS spectra were calibrated according to the C 1s line at 284.8 eV. In order to measure the mass content of active material in the hybrid composites, thermogravimetric analysis (TGA, Pyris 1 TGA, Perkin Elmer) was performed in air from 100 °C to 800 °C at a heating rate of 10 °C min^{-1}.

S-4. Computational Methods

DFT computations were performed using the plane-wave technique implemented in Vienna *ab initio* simulation package (VASP). The projector-augmented plane wave (PAW) approach was applied to describe the ion−electron interactions. The generalized gradient approximation (GGA) expressed by Perdew, Burke and Ernzerhof (PBE)[1] and 500 eV cutoff for the plane-wave basis set were adopted in all computations. The geometry optimizations were performed by using the conjugated gradient method, and the convergence threshold was set to be 10^{-5} eV in energy and 10^{-3} eV/Å in force. The Brillouin zone was sampled with an 8×6×1 centered k-points grid.[2] For the amorphous models, we added some atoms or groups on surfaces randomly, and optimized these models without any constraint. And then, we can get the amorphous surfaces with irregular atoms distribution.

S-5. Supplementary Figures

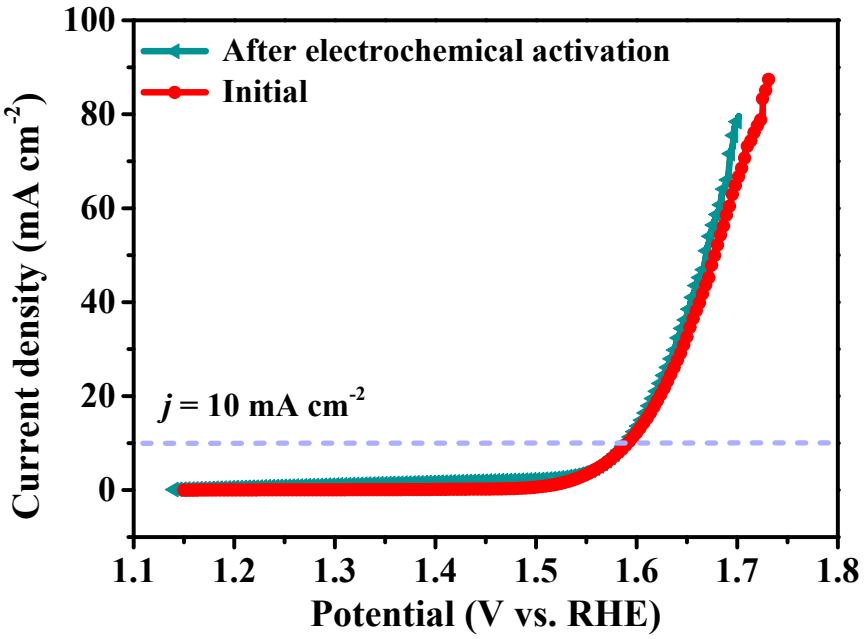

Fig. S1. Polarization curves of $NiFe_2O_4$/NCNF tested in the first cycle and after electrochemical activation process.

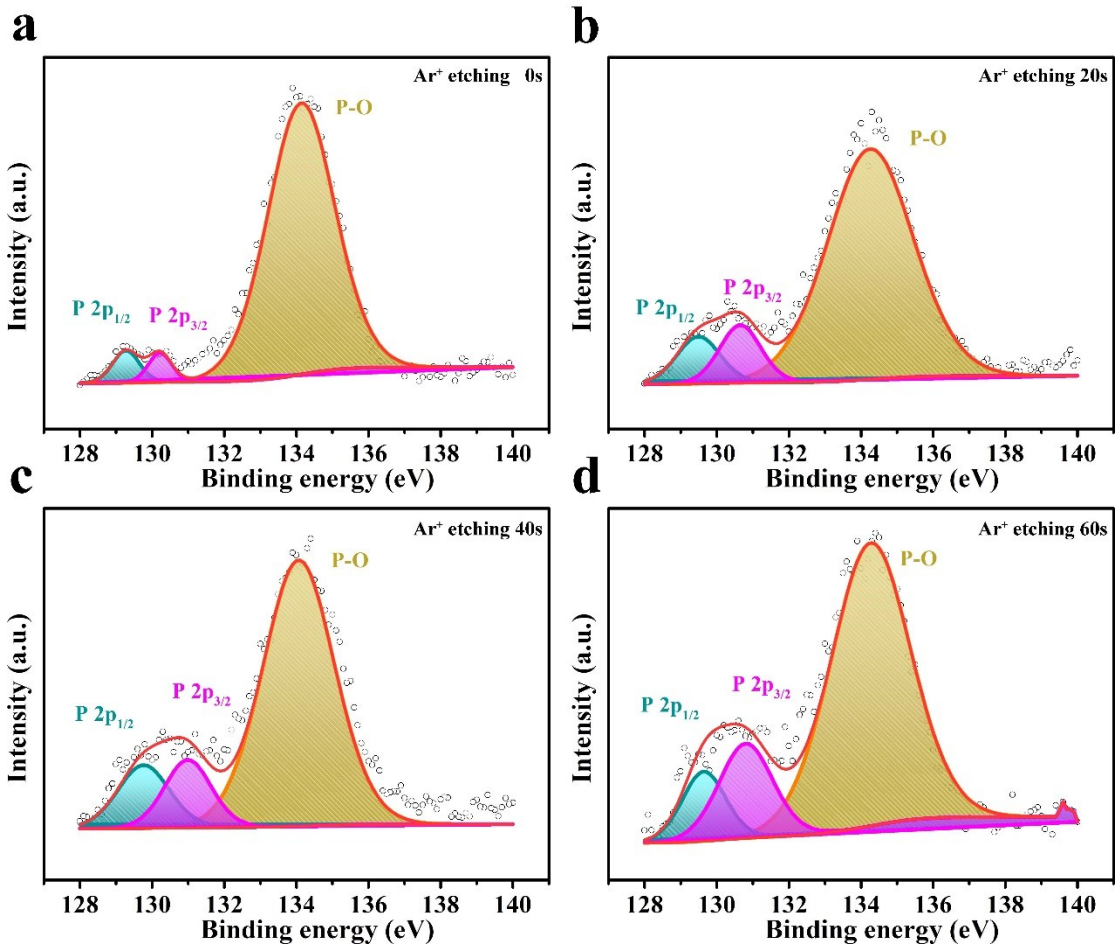

Fig. S2. Depth-profiling P 2*p* spectra of OP-$NiFe_2O_4$/NCNF with different Ar^+ etching time: a) 0, b) 20, c) 40, and d) 60 s.

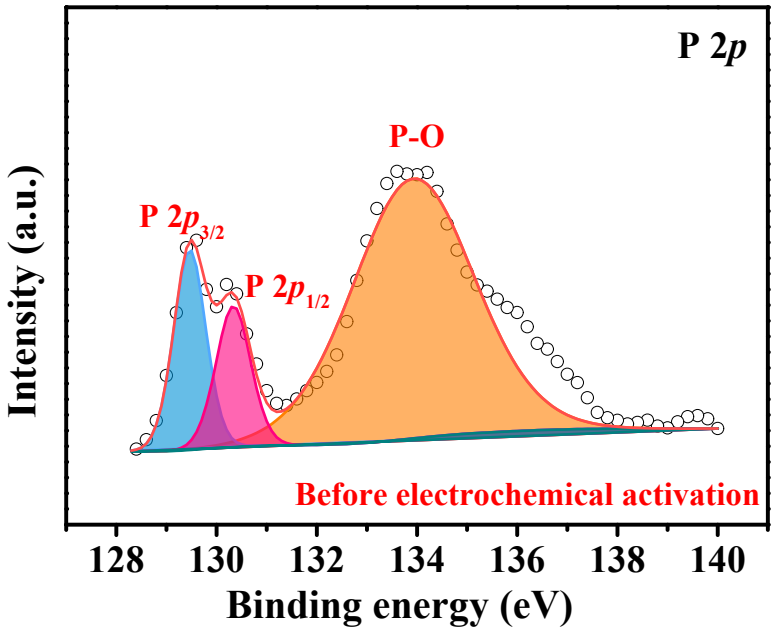

Fig. S3. The P 2*p* spectrum of P-$NiFe_2O_4$/NCNF before electrochemical activation.

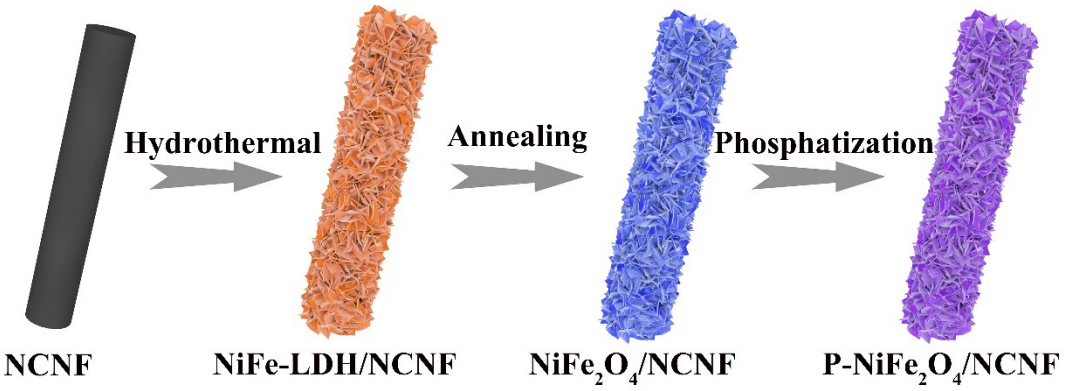

Fig. S4. Schematic illustration of the preparation of P-$NiFe_2O_4$/NCNF composites.

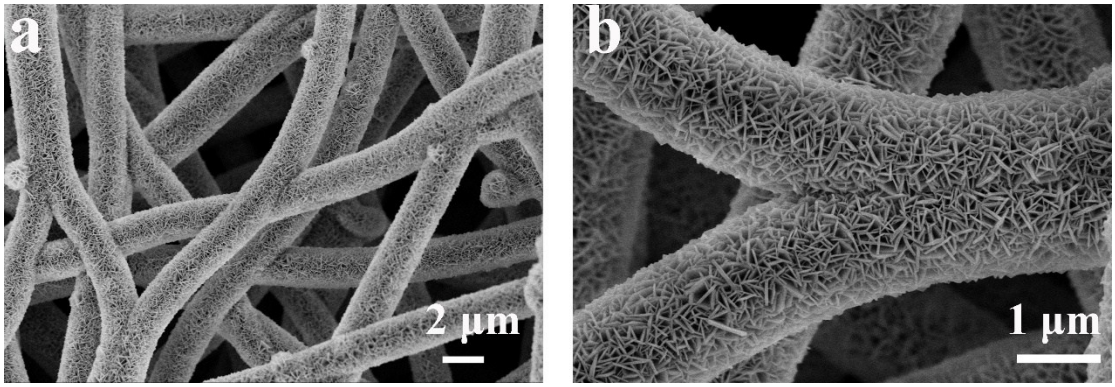

Fig. S5. a, b) FESEM images of NiFe-LDH/NCNF composite with different resolutions.

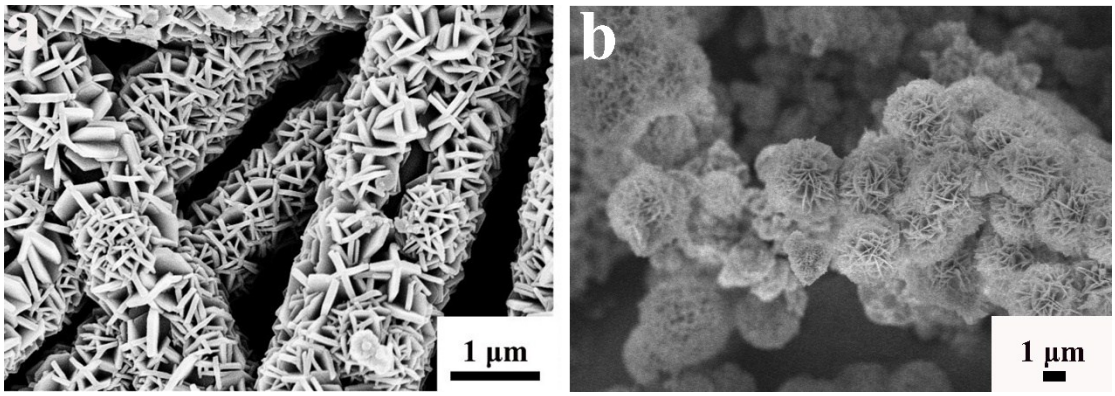

Fig. S6. FESEM images of a) excessive $NiFe_2O_4$ on NCNF, b) the aggregation of $NiFe_2O_4$ powder.

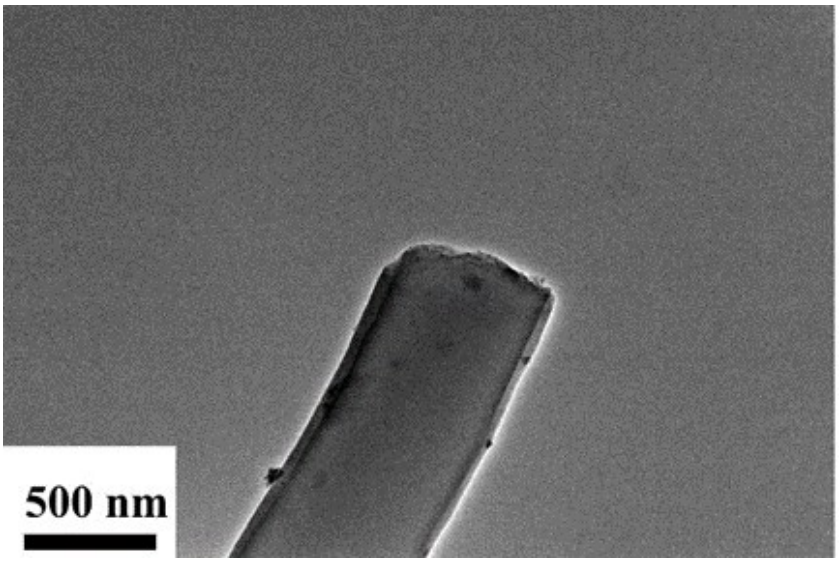

Fig. S7. TEM images of NCNF.

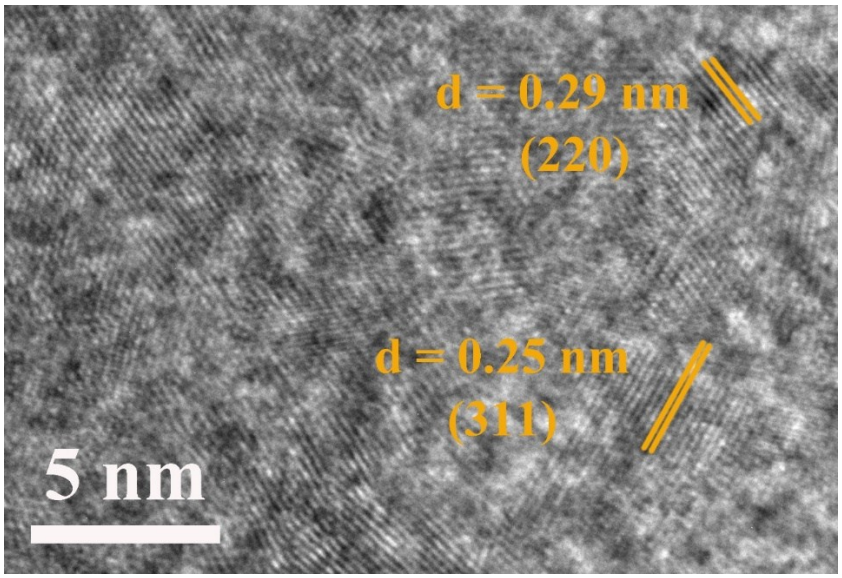

Fig. S8. The HRTEM image of undoped $NiFe_2O_4$/NCNF without stacking faults and distortions.

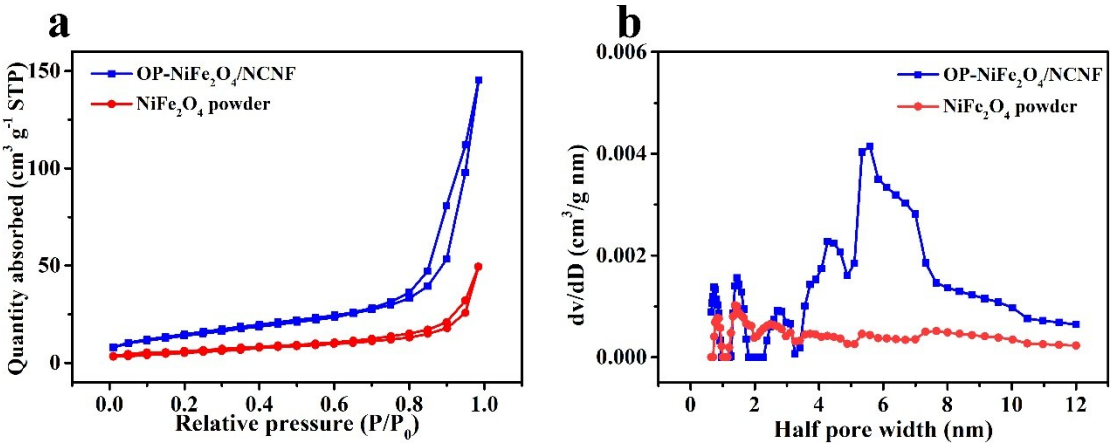

Fig. S9. a) N_2 adsorption–desorption isotherms, and b) the corresponding pore size distribution plots of OP-$NiFe_2O_4$/NCNF and $NiFe_2O_4$ powder.

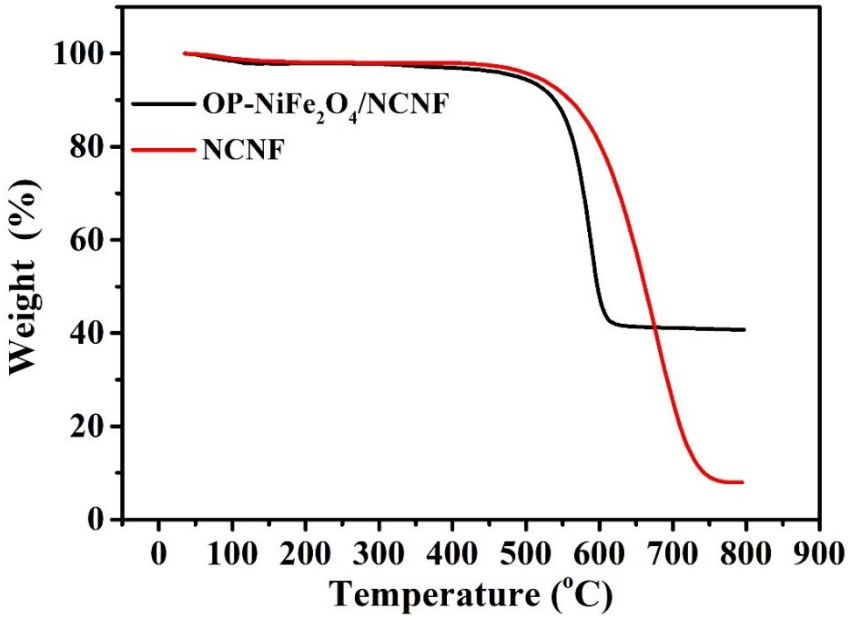

Fig. S10. Thermogravimetric analysis (TGA) profiles of OP-$NiFe_2O_4$/NCNF composite and NCNF.

The weight ratio of OP-$NiFe_2O_4$ nanosheets in OP-$NiFe_2O_4$/NCNF is determined by TGA to be around 35 wt%.

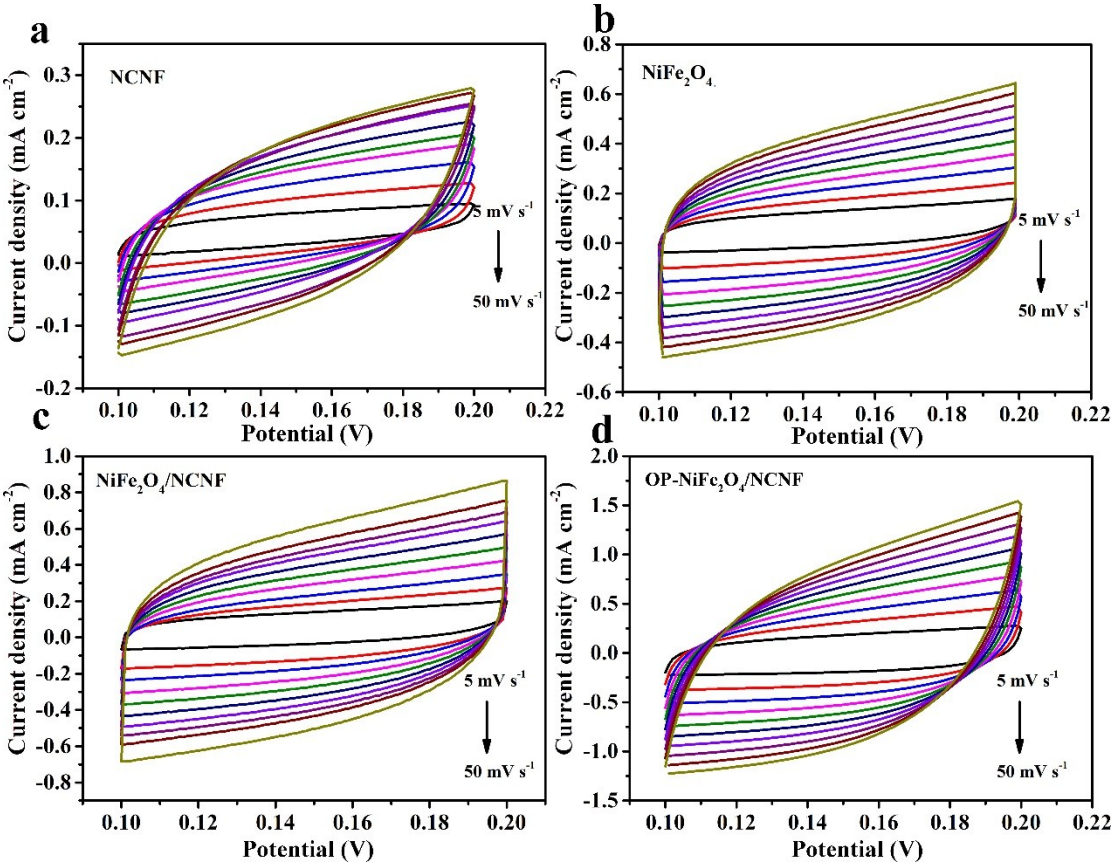

Fig. S11. CV curves of a) NCNF, b) $NiFe_2O_4$, c) $NiFe_2O_4$/NCNF and d) OP-$NiFe_2O_4$/NCNF at different scan rates from 5 to 50 mV s^{-1}.

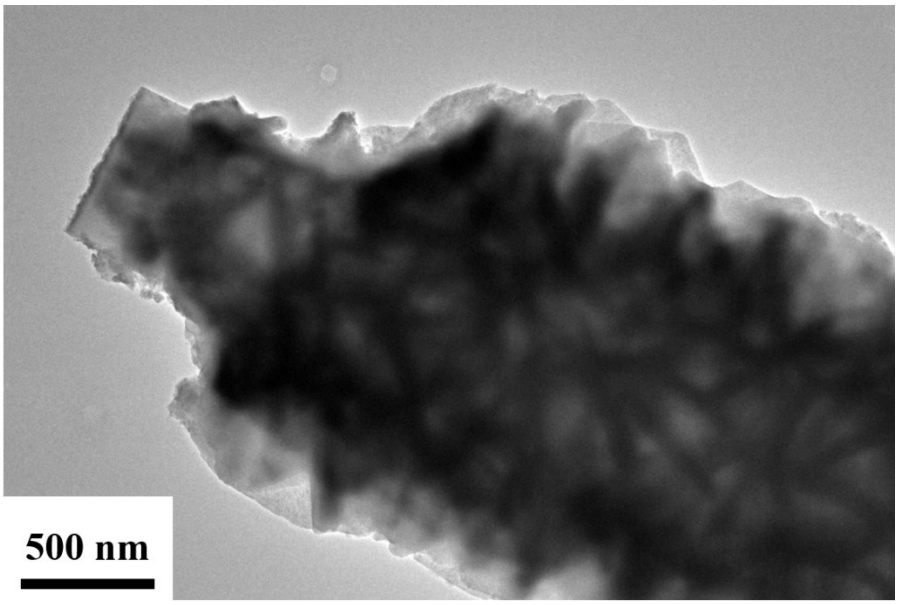

Fig. S12. The TEM of OP-$NiFe_2O_4$/NCNF after 1000 CV cycles.

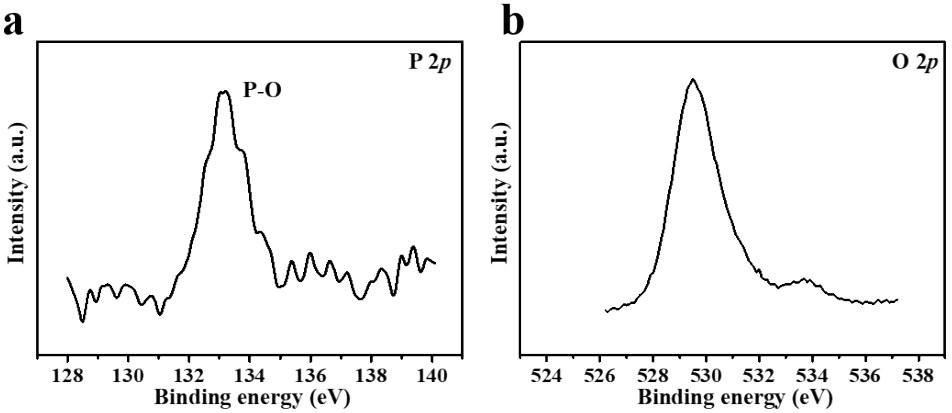

Fig. S13. The XPS of a) P 2*p* and b) O 2*p* in OP-$NiFe_2O_4$/NCNF after 1000 CV cycles.

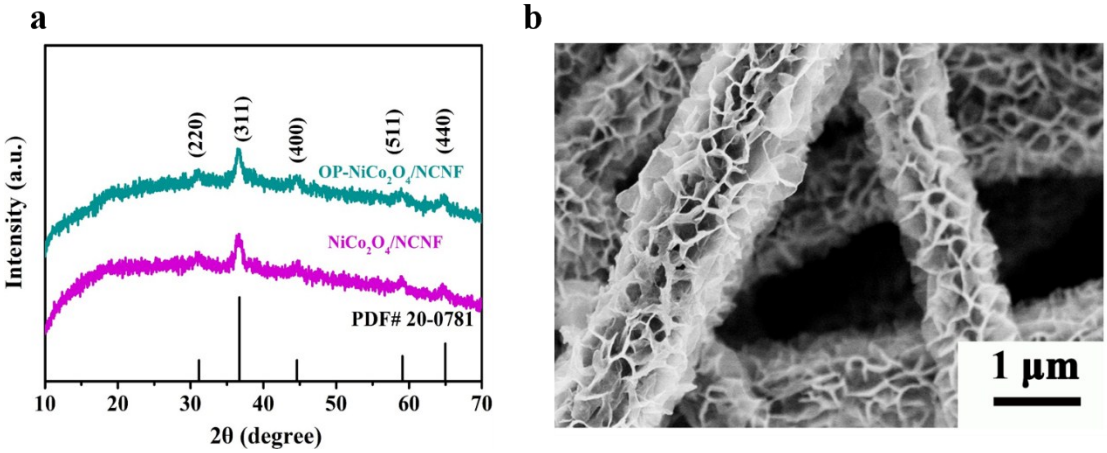

Fig. S14. a) XRD patterns of $NiCo_2O_4$/NCNF and OP-$NiCo_2O_4$/NCNF. b) SEM of OP-$NiCo_2O_4$/NCNF.

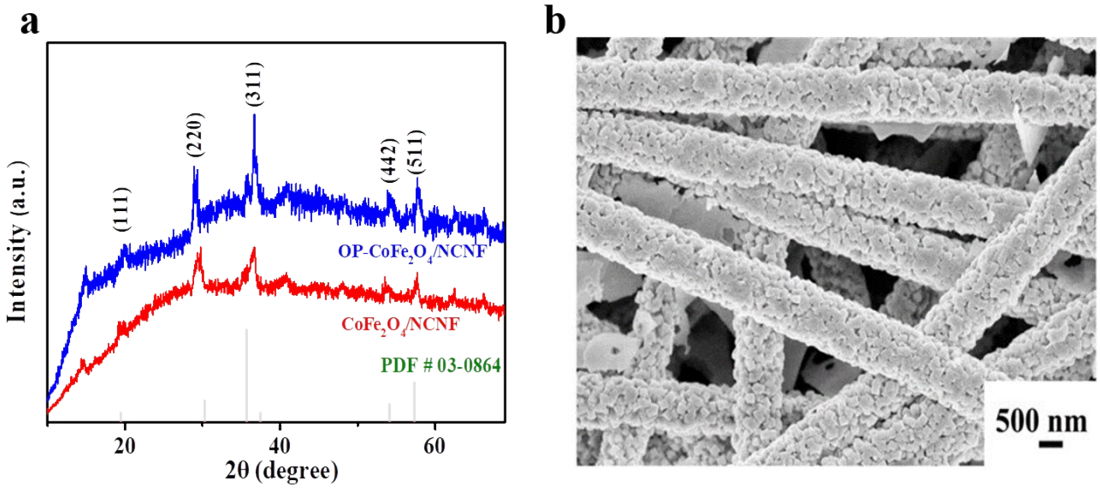

Fig. S15. a) XRD patterns of $CoFe_2O_4$/NCNF and OP-$CoFe_2O_4$/NCNF. b) SEM of OP-$CoFe_2O_4$/NCNF.

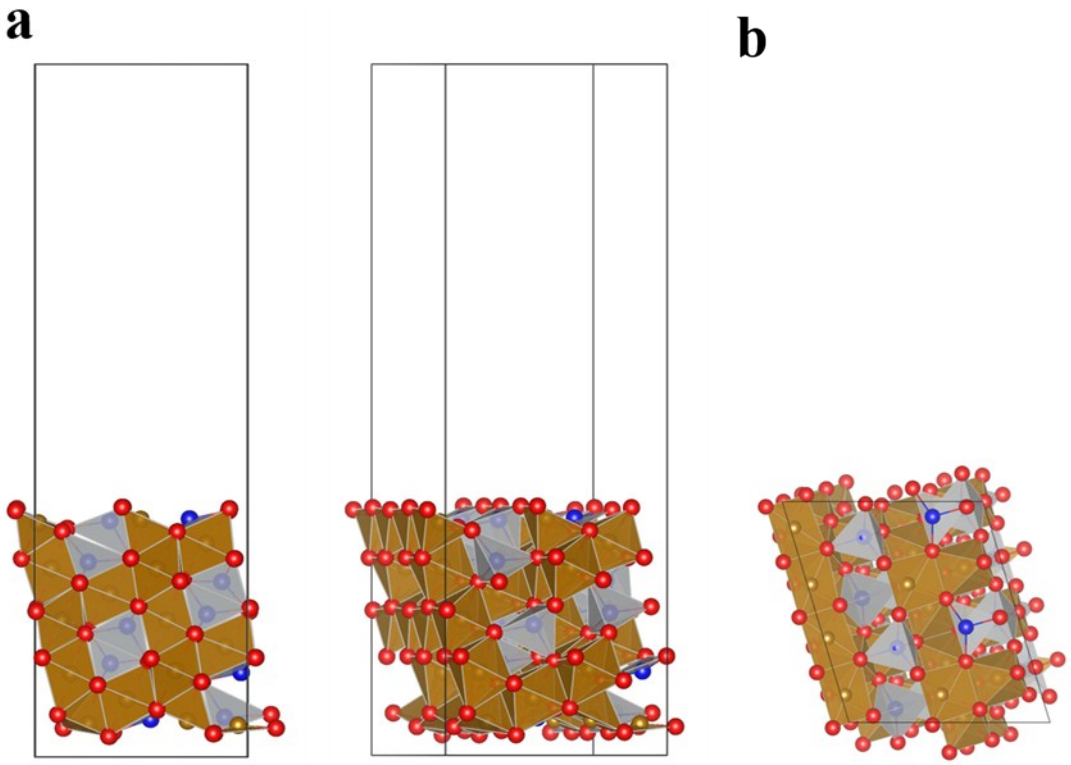

Fig. S16. Crystal models of pristine $NiFe_2O_4$ with different views of a) side view and b) top view.

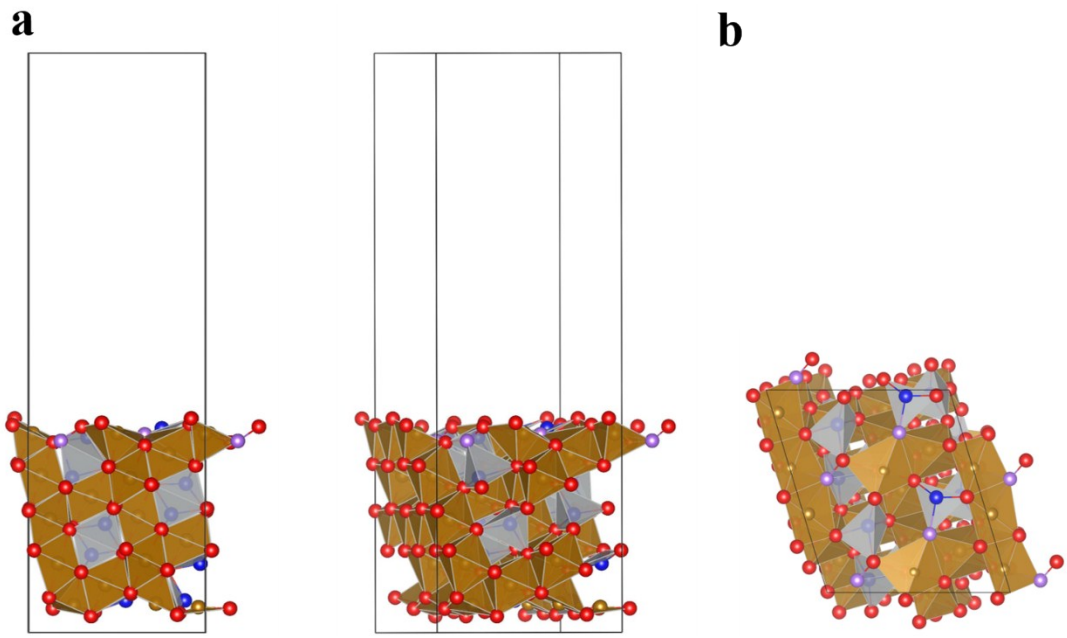

Fig. S17. Crystal models of phosphorus-doped $NiFe_2O_4$ (P-$NiFe_2O_4$) with different views of a) side view and b) top view.

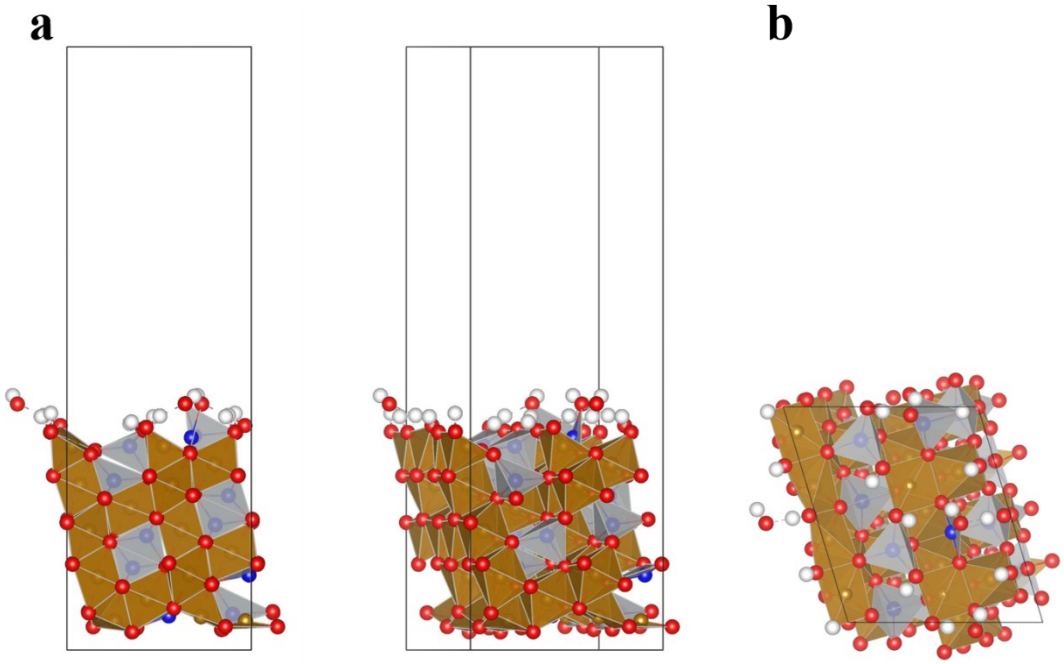

Fig. S18. Crystal models of $NiFe_2O_4$ with amorphous oxyhydroxide layer ($NiFe_2O_4$-OH) of a) side view and b) top view.

S-6. Supplementary Table

Table S1. The P content of OP-$NiFe_2O_4$/NCNF during different Ar^+ etching time.

Sample	P content (%)
OP-$NiFe_2O_4$/NCNF-0s	3.97
OP-$NiFe_2O_4$/NCNF-20s	4.23
OP-$NiFe_2O_4$/NCNF-40s	4.84
OP-$NiFe_2O_4$/NCNF-60s	4.88

Table S2. Comparison of the OER performance of multi-metal oxide catalysts.

Electrode materials	Electrolyte	Current density (mA cm^{-2})	Overpotential vs. RHE (mV)	Tafel slope (mV dec^{-1})	Ref
$NiCo_2O_4$ nanoneedles	1 M KOH	10	323	292	[3]
$ZnCo_2O_4$	1 M KOH	10	390	46	[4]
Spindle-like $ZnCo_2O_4$	1 M KOH	10	389	59.5	[5]
$Zn_{0.45}Co_{2.55}O_4$	1 M KOH	10	330	39	[6]
$NiFe_2O_4$	1 M KOH	10	360	40	[7]
$MnCo_2O_4$	1 M KOH	10	530	85	[8]

$CoFe_2O_4$	1 M KOH	10	330	75	[9]
$NiFe_2O_4$ NF	1 M KOH	5	470	98.2	[10]
Fe–Ni hydroxide/graphitic mesoporous carbon	1 M KOH	10	320	57	[11]
Defect-rich ultrathin Co–Fe LDH	1 M KOH	10	300	58	[12]
$Ni_{1-x}Fe_xO$	0.5 M KOH	10	325		[13]
CoV_2O_6–V_2O_5/NRGO-1	1 M KOH	10	239	49.7	[14]
SnCoFe-Ar	1 M KOH	10	270	42.3	[15]
MnO_2/$NiCo_2O_4$/NF	1 M KOH	10	340	139	[16]
OP-$NiFe_2O_4$/NCNF	1 M KOH	10	260	44.8	This work

S-7. References

[1] J. P Perdew, K. Burke, M. Ernzerhof. *Rev*. *Lett*., 1996 **77**, 3865-3868.
[2] H. J Monkhorst, J. D Pack, *Phys*. *Rev*. *B*., 1976 **13**, 5188-5192.
[3] H. Shi, G. Zhao, *J*. *Phys*. *Chem. C,* 2014, **118**, 25939-25946.
[4] T. W Kim, M. A Woo, M. Regis, K. S Choi, *J. Phys. Chem. Lett.,* 2014, **5**, 2370-2374.
[5] J. Zhang, D. Zhang, Y. Yang, J. Ma, S. Cui, Y. Li, B. Yuan, *RSC. Adv.*, 2016, **6**, 92699-92704.
[6] S. Han, S. Liu, R. Wang, X. Liu, L. Bai, Z. He, *ACS Appl. Mater. Interfaces.,* 2017, **9**, 17186-17194.
[7] J. Landon, E. Demeter, N. Inoglu, C. Keturakis, I. E Wachs, R. Vasić, A. I Frenkel, J. R Kitchin, *ACS Catal.,* 2012, **2**, 1793-1801.
[8] C. Xu, M. Lu, Y. Zhan, J. Y Lee. *RSC Adv.,* 2014, **4**, 2508-25092.
[9] P. Li, R. Ma, Y. Zhou, Y. Chen, Z. Zhou, G. Liu, Q. Liu, G. Peng, Z. Liang, J. Wang, *J. Mater. Chem. A*, 2015, **3**, 15598-15606.
[10] M. Li, Y. Xiong, X. Liu, X. Bo, Y. Zhang, C. Han, L. Guo. *Nanoscale,* 2015, **7**, 8920-8930.
[11] L. Wang, X. Huang, J. Xue. *ChemSusChem,* 2016, **9**, 1835-1842.
[12] P. F Liu, S. Yang, B. Zhang, H. G Yang, *ACS Appl. Mater. Interfaces*, 2016, **8**, 34474-34481.
[13] A. C. Pebley, E. Decolvenaere, T. M. Pollock, M. J. Gordon, *Nanoscale,* 2017, **9**, 15070-15082.
[14] G. Shen, L. Wang, N. Mahmood, L. Pan, W. Xu, M. A. Qadeer, I. Aslam, X. Zhang, M. Tahir, Y.-C. Wang, R. Zhang, J.-J. Zou, *ACS Energy Lett.,* 2017, **2**, 1327-1333.
[15] D. Chen, M. Qiao, Y.-R. Lu, L. Hao, D. Liu, C.-L. Dong, Y. Li, S. Wang, *Angew. Chem., Int. Ed.,* 2018, **57**, 8691-8696.
[16] K.-L. Yan, X. Shang, W.-K. Gao, B. Dong, X. Li, J.-Q. Chi, Y.-R. Liu, Y.-M. Chai, C.-G. Liu, *J. Alloys Compd*., 2017, **719**, 314-321.